Catalysis Today 150 (2010) 16–21

Contents lists available at ScienceDirect

Catalysis Today

journal homepage: www.elsevier.com/locate/cattod

Performance of carbon nanofibres, high surface area graphites, and activated carbons as supports of Pd-based hydrodechlorination catalysts

Ruben F. Bueres, Esther Asedegbega-Nieto, Eva Díaz, Salvador Ordóñez *, Fernando V. Díez

Department of Chemical Engineering and Environmental Technology, University of Oviedo, Julián Clavería s/n, 33006 Oviedo, Spain

ARTICLE INFO

Article history:
Available online 25 June 2009

Keywords:
Tetrachloroethylene
Hydrodechlorination
Pd catalyst
Carbon nanofibres
High surface area graphites

ABSTRACT

Palladium catalysts (1 wt%) supported on three different carbonaceous supports (activated carbon, AC; carbon nanofibre, CNF; and high surface area graphite, HSAG) were prepared and tested for tetrachloroethylene (TTCE) catalytic hydrodechlorination at 523 K and 195 h^{-1} space velocity (WHSV). Organic solutions (0.9 mol/L of TTCE in toluene) were used as feed, simulating real chlorinated wastes. Pd/activated carbon and Pd/CNF have shown a fast deactivation on stream, whereas the HSAG-supported catalyst showed the best performance. Characterization of fresh and used catalysts by BET, TEM, XRD and XPS revealed that the deactivation of Pd/AC catalyst is caused by the micropore blockage because of coke formation, whereas in the case of Pd/CNF, deactivation is caused by a combination of coke deposition (in lower extent than in the case of activated carbon), active phase sintering and chlorine poisoning. The best behaviour of the HSAG-based catalysts is caused by the absence of sintering and coke formation, although chlorine poisoning is still present.

1. Introduction

Organochlorinated wastes are commonly generated in many dry-cleaning and textile modern installations. Specifically, tetrachloroethylene (TTCE) is used in most cases as solvent, generating wastes containing high TTCE concentrations (up to 40%) and other hydrocarbons. This waste (viscous liquid or solid, depending on the operation conditions), which is water-insoluble and very soluble in organic solvents, is considered as a hazardous waste because of its high TTCE content [1,2]. Catalytic hydrodechlorination (HDC), which consists of treating the chlorinated compound with hydrogen in order to transform it into hydrocarbons and hydrogen chloride (easily absorbed in water or alkali), could be a safe alternative for the treatment of these wastes [3].

Among the catalysts proposed for the hydrodechlorination of TTCE in organic wastes, palladium catalysts are considered the most active ones [4,5]. It is also fully accepted that catalyst support plays a key role on both catalytic activity and stability. Previous studies on Pd supported catalysts on activated carbon conclude that the main deactivation cause is the catalyst fouling caused by formation of coke deposits, blocking the micropores of the activated carbon [6]. However, the activated carbon supported catalysts showed an initial conversion 40% higher than the alumina-supported ones for the same palladium loading, attributed to the best dispersion of the active phase and the spill-over phenomena, that increases the adsorption of the reactant on the catalyst [6,7]. Concerning the inorganic supports (such as γ-Al_2O_3), they present also important drawbacks, such as high sensibility to the hydrogen chloride generated in the reaction or the catalysis of undesired side reactions by the support acid sites [8].

Therefore, non-microporous carbons, such as carbon nanofibres (CNFs) and high surface area graphites (HSAGs), are receiving increasing attention as catalyst supports [9–12]. Its non-microporous character suggests that coke formation (only catalysed by the active metal) might not deactivate these catalysts as dramatically as it occurs with Pd/AC, and its carbonaceous character confers them high resistance to hydrogen chloride poisoning and high affinity for organic compounds. In this way, Amorim et al. [9] studied the hydrodechlorination of chlorobenzene over CNF-supported palladium catalysts, among other materials, whereas Liu et al. reported an enhanced activity of Pd/CNF when they were treated with gaseous ammonia [10]. All these works were carried out with diluted organochlorinated-hydrogen mixtures, whereas in the industrial practice the chlorinated compounds are usually dissolved in an organic matrix, or as a solid or sludge that must be dissolved before treatment (as the procedure followed in the experiments reported in this work). On the other hand, the performance of HSAG as support for hydrodechlorination catalysts has not been, to the best of our knowledge, studied yet.

In this work, palladium supported on CNF and HSAG were compared to the more conventional Pd/activated carbon for the

* Corresponding author. Tel.: +34 985 103 437; fax: +34 985 103 434.
E-mail address: sordonez@uniovi.es (S. Ordóñez).

0920-5861/$ – see front matter © 2009 Elsevier B.V. All rights reserved.
doi:10.1016/j.cattod.2009.05.020

hydrodechlorination of TTCE in organic matrix (toluene). Catalyst deactivation was studied, and fresh and used catalysts were characterized by different techniques in order to determine the deactivation causes.

2. Experimental

2.1. Catalysts preparation

The supports of the catalysts tested in this study are commercially available carbonaceous materials. Activated carbon (GF-40) was supplied by Norit (The Netherlands), CNFs (Pyrograf III, PR-24 HHT) by Applied Sciences (Ohio, USA) and high surface area graphite (HSAG 300) by TIMCAL (Bodio, Switzerland). All the materials were used as purchased. In all the cases, a high purity carbonaceous material was chosen, avoiding the presence of transition metals.

Palladium catalysts were prepared by the wet impregnation method using $PdCl_2$ as precursor, with a nominal palladium loading of 1 wt%. The impregnation solution consisted of $PdCl_2$ dissolved in 0.1N HCl to generate H_2PdCl_4, with a solution volume exceeding by 20% the pore volume of the support in each case. This precursor solution was dissolved in 60 cm^3 of 0.1N HCl. One gram of the carbonaceous support was added to this solution in a flask under magnetic stirring for 10 min. The flask was then placed in a rota-vapor equipped with a water bath at 343 K, spun and vacuum pumped for 0.5 h. Next, the powder was dried in a stove at 383 K for 2 h. Finally, in order to avoid mass-transfer limitations and pressure gradients inside the catalytic bed, the catalysts obtained were pelletized (applying two successive cycles at 9.8×10^4 N for 30 s each one), crushed, and sieved to particle sizes within the range of 63–100 μm.

2.2. Reaction studies

The gas phase HDC of TCE at 523 K and 0.5 MPa was carried out in a fixed-bed reactor (WHSV = 195 h^{-1}), with a great excess of hydrogen (90:1, molar) to ensure that it is not a limiting reactant. In previous works with palladium catalysts, deactivation effects were detected at this temperature [6,7]. More details about the catalytic reactor and operating conditions are given elsewhere [13]. Before the catalytic tests, the catalysts were activated in situ by passing through the reactor 0.60 L/min (s.t.p.) of hydrogen at 523 K and 0.5 MPa for 2.5 h. The organic feed (toluene as solvent and tetrachloroethylene, both supplied by Panreac with a minimum purity of 99.5 and 99.9%, respectively) flowed downwards through the reactor, being completely vaporized at reaction conditions. Reaction products were condensed and analyzed by capillary GC in a Shimadzu GC-2010 apparatus equipped with a FID detector, using a 15 m long WCOT silica-fused capillary column as stationary phase. Peak assignment was performed by GC–mass spectra and responses were determined using standard calibration mixtures, being analytical repeatability better than ±0.2%. Non-condensed gases were absorbed in alkaline solution, followed by chloride titration using the Mohr method. Conversion has been calculated in terms of the concentration of tetrachloroethylene in the liquid feed ($C_{TTCE,0}$) and in the condensed reactor outlet (C_{TTCE}) as $[(C_{TTCE,0} - C_{TTCE})/C_{TTCE,0}]$, and trichloroethylene selectivity has been calculated as mole of trichloroethylene released per mole of tetrachloroethylene reacted $[C_{TCE}/(C_{TTCE,0} - C_{TTCE})]$. Since ethane and trichloroethylene are the only reaction products, the selectivity for ethane formation is calculated as $[1 - C_{TCE}/(C_{TTCE,0} - C_{TTCE})]$. The yield for total dechlorination has been calculated as the product of the tetrachloroethylene conversion by the selectivity for ethane formation. Chlorine mass balance was checked in order to ensure the absence of other undetected chlorinated compounds, with balance closures higher than 95% in all cases.

2.3. Catalysts characterization

The textural characterization of the materials (specific surface area and pore volume) was based on N_2 adsorption isotherms, determined with a Micromeritics ASAP 2000 surface analyzer. Powder X-ray diffraction (XRD) was performed with a Philips PW1710 diffractometer, working with the Cu Kα line (λ = 0.154 nm). Measurements were carried out in the range of 2θ 35–45°, at a scanning rate of 0.002° in 2θ min^{-1} in order to study the active metal, as the (1 1 1) crystallographic plane of Pd diffract the X-ray beam at 40.1°. Likewise, the Pd particle morphology and size distributions were determined by transmission electron microscopy (TEM), a JEOL JEM2000EXII microscope.

Carbonaceous deposits on the catalysts after reaction were characterized by temperature-programmed oxidation (TPO), employing a Micromeritics TPD-2900 apparatus connected to a Pfeiffer Vacuum-300 mass spectrometer. For this purpose, 10 mg carbon samples were maintained in an oxygen-stream – 2% O_2/98% He – at 50 °C for 30 min, with a flow rate of 50 cm^3 min^{-1}, and heated from 323 to 373 K at 10 K min^{-1}.

The chemical composition of the fresh and used catalysts was determined by X-ray photoelectron spectroscopy (XPS). XPS experiments were carried out in a SPECS system equipped with a hemispherical electron analyzer operating in a constant pass energy, using Mg Kα radiation ($h\nu$ = 1253.6 eV). The samples were fixed to the sample holder using a carbon adhesive tape. The background pressure in the analysis chamber was kept below 2×10^{-9} mbar during data acquisition. Since samples are conductor (confirmed on observing the position of the C 1s peak at 284.6 eV), there was no need of applying surface neutralization during measurements.

3. Results and discussion

3.1. Characterization of fresh catalysts

The measured BET surface area and pore volume of the studied catalysts are shown in Table 1. The activated carbon catalyst exhibits the highest surface area due to its microporous character, although an important decrease was observed after the impregnation (37.5%). A similar reduction (31%) in surface area was observed for the HSAG-supported catalyst, decreasing the mesopore volume from 0.46 to 0.29 cm^3 g^{-1}. Concerning the Pd/CNF, its surface area does not vary significantly after the impregnation with Pd, maintaining also the volume of mesopores at 0.16 cm^3 g^{-1}. In all cases, the adsorption isotherms of the Pd catalysts present the same shape as the parent materials [14].

The XPS surface analysis shows that the Pd content is very close to the nominal loading (1 wt%) in all cases. Both Pd and Pd^{2+} species are found after the reduction, with Pd^{2+}/Pd ratio around 0.25 for the three catalysts (Table 1). TEM images provided in Fig. 1 illustrate the Pd particle morphology and dispersion on the three carbon catalysts. The Pd/activated carbon catalyst exhibits a globular geometry, with a certain trend to form particle agglomerates, which could be caused by a limited metal–support interaction [9]. Palladium particles on CNF and HSAG present lower

Table 1
Physicochemical characterization of the three carbon supported Pd catalysts.

	Pd/AC	Pd/CNF	Pd/HSAG
S_{BET} (m^2 g^{-1})	1069	32	222
$V_{mesopores}$ (cm^3 g^{-1})	0.36	0.16	0.46
d_{XRD} (nm)	42	31	25
d_{TEM} (nm)	53	16	5

size. This trend agrees with the estimated particle size determined from TEM images (at least 150 measured particles), and with the average diameter obtained from the Scherrer formula to the XRD peak 1 1 1 of Pd (Table 1). The differences in mean particle sizes obtained by both the techniques are remarkable, especially for CNF and HSAG supports, where the average particle size obtained for TEM is 51 and 28% the one obtained by XRD, respectively. These differences in the Pd mean particle size were also reported in the literature for carbon based materials [15,16]. In our case the case of Pd/HSAG is especially remarkable, which can be explained taking into account that the crystallite size obtained by TEM is within the range of the detection limit of XRD, thus one can expect inaccurate results from this technique.

3.2. Reaction studies

The hydrodechlorination of TTCE over the three catalysts generated ethane as main product and trichloroethylene as the only chlorinated intermediate, according to the reactions:

$$C_2Cl_4 + H_2 \rightarrow C_2HCl_3 + HCl \quad (1)$$

$$C_2HCl_3 + 4H_2 \rightarrow C_2H_6 + 3HCl \quad (2)$$

The closure of the chlorine mass balance was better than 95% in all cases. The solvent (toluene) was partially hydrogenated in the first hours on stream, yielding methyl-cyclohexane (MCH). Evolution of TTCE conversion and selectivity for the three studied catalysts are shown in Fig. 2. The yields for the total hydrodechlorination of the feed for the studied catalysts (mole of non-chlorinated product formed per mole of TTCE fed) are depicted in Fig. 3. The HSAG-supported catalyst presents the highest initial TTCE conversion (97%), followed by Pd/CNF (70%) and Pd/AC (68%). For times on stream higher than 30 h the difference among the graphite supported catalyst and the others increases, the conver-

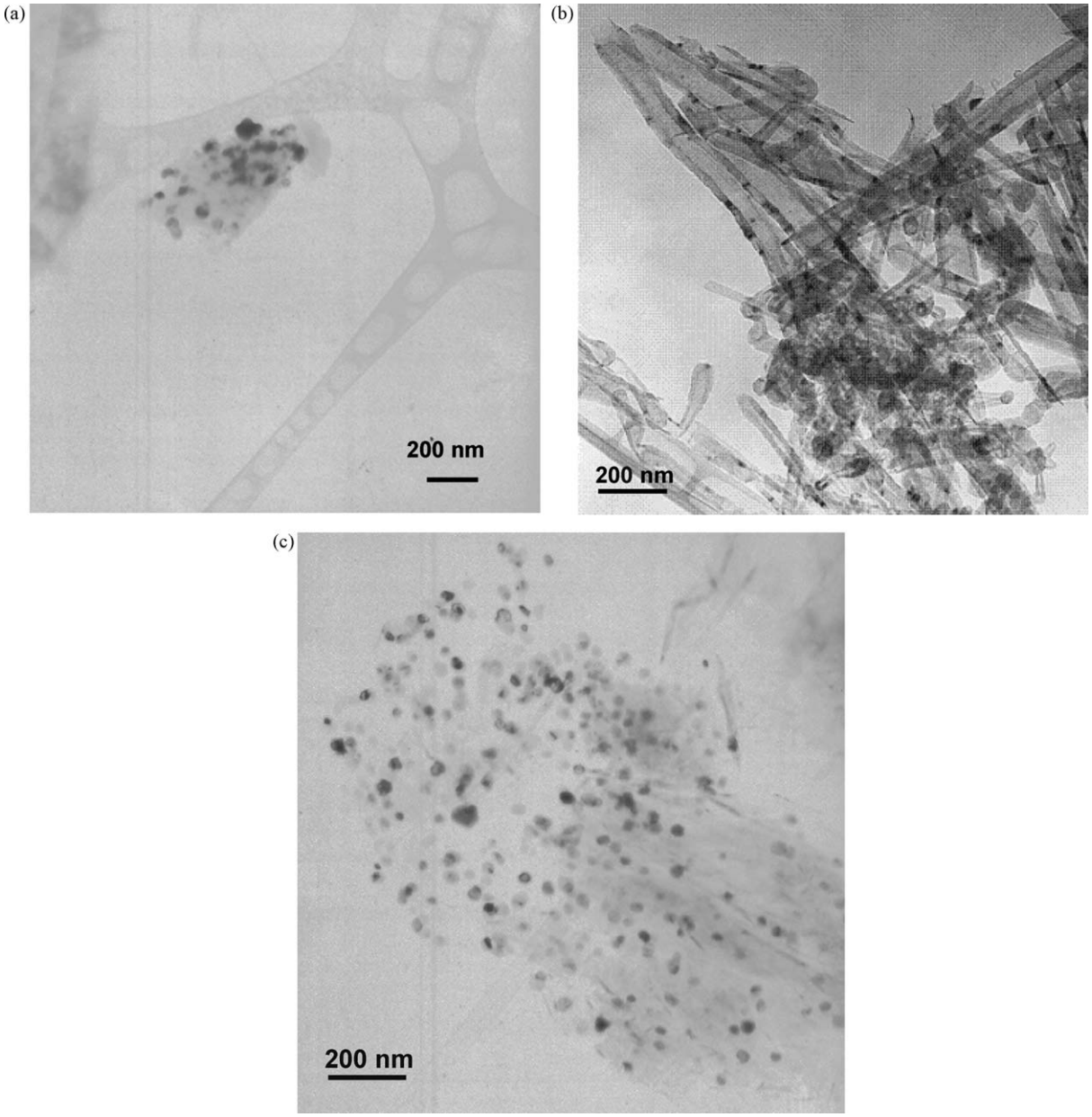

Fig. 1. TEM images of (a) 1%-Pd/AC, (b) 1%-Pd/CNF and (c) 1%-Pd/HSAG.

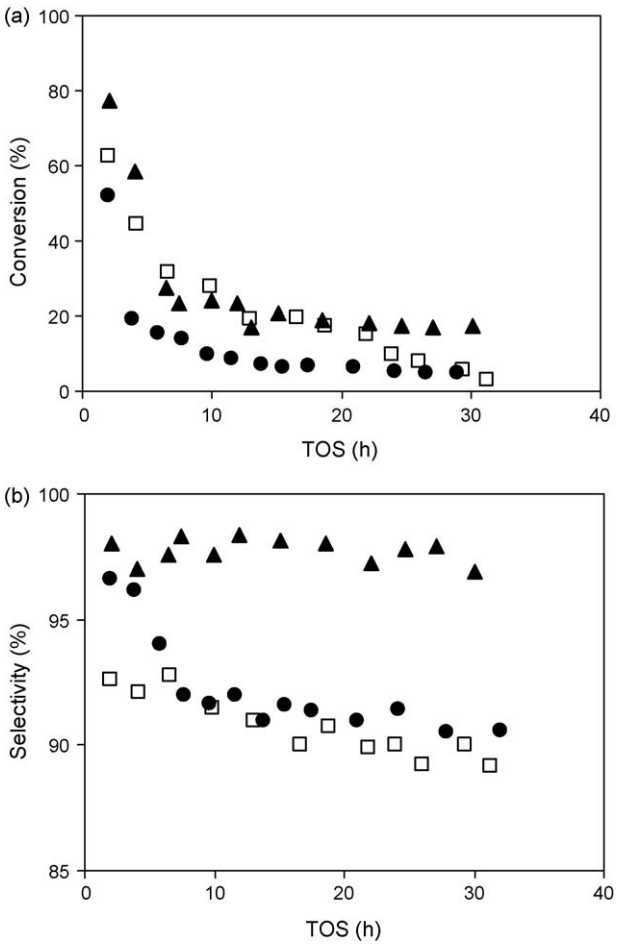

Fig. 2. Evolution of (a) TTCE conversion and (b) selectivity for ethane formation, with the time on stream for: Pd/AC (□), Pd/HSAG (▲) and Pd/CNF (●).

sion provided by the HSAG catalyst being up to three times the one obtained with the other catalysts. Concerning the selectivity, for the HSAG catalyst it is higher than 95% during all the experiments, whereas for Pd/CNF, selectivity drops sharply during the first 4 h, and then more gradually. In the case of Pd/AC, the selectivity shows a gradual decreasing trend, dropping to 89% at the end of the experiment.

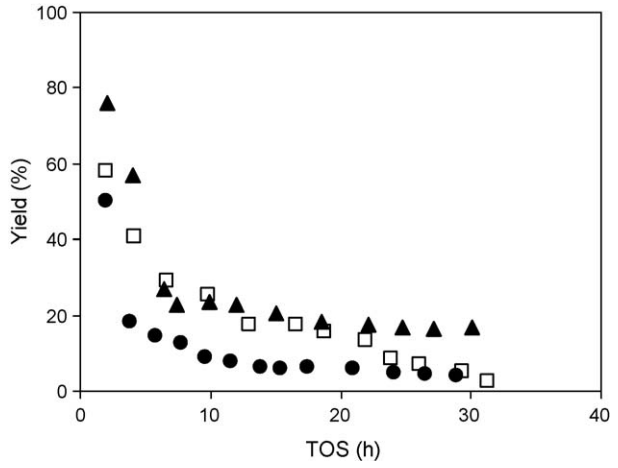

Fig. 3. Evolution of the total hydrodechlorination yield (mole of ethane formed per mole of TTCE fed to the reactor, in percentage). See Fig. 2 caption for notation.

The Pd/AC loss of activity with time on stream was also observed in the literature, both for gas phase [6,9,10] and liquid phase [17] hydrodechlorination, and was attributed to carbon deposition on the active phase and chlorine poisoning. Although for short time on stream, Pd/CNF shows lower conversion and higher selectivity than Pd/AC, for higher time on stream the activity and selectivity provided by both catalysts are similar. The slower deactivation of Pd/HSAG vs. Pd/AC contrasts with the results reported in the literature [9], where a Pd supported catalyst on graphite deactivated much faster than the activated carbon supported one. This different behaviour can be caused by the different chemical nature of HSAG and conventional graphite [18]. Functional groups (carbonyl and carboxyl groups) present in HSAG but not in graphite, can act as HCl sinks, minimising the poisoning of the active phase. Overall, Pd/HSAG shows the best performance, as shown in Fig. 3, where the yield to total dechlorination for the three catalysts is compared. This could be explained by the HSAG morphology, constituted by flat graphene layers, with a quite irregular morphology and several pore diameters, which favour the transport processes between the active sites and the gas phase [11]. In the case of the CNF-supported catalyst, the graphene layers are stacked, thus decreasing the exposed area. The difference in selectivity could be attributed to several factors: (i) the existence of metal–support interactions between the Pd crystallites and the HSAG surface, which induce high dispersion of the active phase (Table 1), and could facilitate the spill-over phenomena or the mass-transfer of H_2 to the catalytic active sites, hence favouring the reaction [19]; (ii) the complete absence of microporosity as found on the activated carbon, which could modify the residence time of the reactants and products and their adsorption properties [20]; and (iii) the presence of a certain amount of surface oxygen groups on HSAG [21], by contrast with CNF [22]. In this way, Toebes et al. [23] found that the presence of oxygenated groups favoured the fully hydrogenation of cinnamaldehyde, whereas the absence of these groups was related to the selective hydrogenation of C=C bonds.

3.3. Characterization of the used catalysts

In order to gain further understanding on the deactivation behaviour, aged catalysts (after 35 h on stream) were characterized with different instrumental techniques. BET results showed that the Pd/AC catalyst exhibits a decrease in surface area to 600 $m^2\,g^{-1}$, whereas no appreciable morphological changes were observed for neither CNF nor HSAG supports. Surface analysis (XPS) of the catalysts did not reveal any decrease in Pd concentration during the reaction.

For the Pd/HSAG catalyst, the average crystallite size shows no appreciable differences after reaction, with an average size (TEM) of 5 nm – the active phase in the used Pd/HSAG catalyst has not been observed by XRD. However, both AC- and CNF-supported catalysts show an important sintering effect, according to XRD measurements, their particle size increasing to 90 and 52 nm, respectively. There is a good correlation between sintering and the activity loss of the catalysts, since the activated carbon catalyst presented the most pronounced deactivation, whereas Pd/HSAG exhibited the highest stability on stream. In this way, the absence of functional groups on the CNF catalyst could lead to a very weak interaction of the metal particles with the support, increasing the probability of crystallite coalescence.

XRD patterns showed a displacement of the Pd main peak to a lower scattering angle after reaction for AC and CNF supports. This displacement was attributed in the literature [24,25] to the formation of palladium carbide from carbonaceous deposits on the metal surface. The existence of these carbonaceous deposits was more deeply studied by TPO analyses. In agreement with XRD

Table 2
Main XPS parameters obtained for the fresh and used catalysts used in this work: Pd/C ratio, binding energies of the different Pd and chlorine species and Cl/Pd ratio.

Catalysts	Pd $3d_{5/2}$				Cl $2p_{3/2}$		Cl/Pd
	XPS mass ratio (Pd/C)	BE Pd^0 (eV)	BE Pd^{2+} (eV)	Ratio Pd^{2+}/Pd^0	BE Cl^-, eV (%)	BE C–Cl bond, eV (%)	
Pd/AC (fresh)	1.08	335.5	338.0	0.25	198.6 (40.0)	200.1 (60.0)	1.5
Pd/AC (used)	1.01	335.2	337.7	2.17	198.5 (18.9)	200.4 (81.1)	5.0
Pd/CNF (fresh)	1.02	335.7	338.0	0.22	198.6 (65.8)	200.0 (34.2)	1.0
Pd/CNF (used)	0.85	335.2	337.6	2.27	198.6 (20.8)	200.6 (79.2)	9.6
Pd/HSAG (fresh)	1.20	334.7	338.1	0.58	198.7 (41.8)	200.0 (58.2)	2.4
Pd/HSAG (used)	1.01	335.6	338.0	2.71	198.0 (40.5)	199.4 (59.5)	4.1

results, AC and CNF used catalysts showed two peaks for the CO_2 evolved. The main peak, at around 780 and 1030 K for Pd/AC and Pd/CNF, respectively, corresponds to the combustion of the carbon supports, whereas the second peak (at around 610 and 670 K, respectively) is related to the burning of carbonaceous deposits [6]. For the used Pd/HSAG catalyst, only the decomposition of the support at about 1070 K was observed.

The percentage of coke per weight of catalyst, determined from the area of the peaks, was 3.5 and 1.70% for Pd/AC and Pd/CNF, respectively. Coke decomposes at lower temperature over the activated carbon catalysts, since the organic functional groups of the support may catalyse the combustion, whereas in the case of the more inert CNFs this effect does not take place.

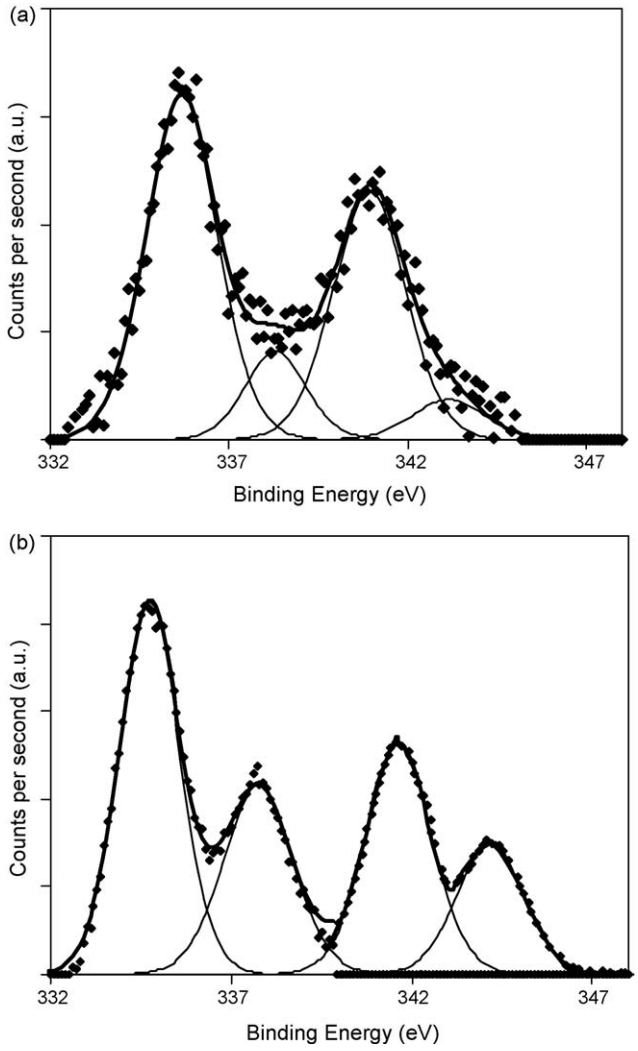

Fig. 4. Pd 3d core-level spectra of: (a) Pd/CNF and (b) Pd/HSAG.

In order to get more information on the catalyst deactivation causes, XPS surface analyses of the fresh and used catalysts were performed. Data of the XPS parameters for Pd $3d_{5/2}$ and Cl $2p_{3/2}$ core levels of both the fresh and used catalysts are summarized in Table 2. The original Pd 3d core-level spectra for the fresh catalysts, and the fit of the curves, shown in Fig. 4, reveal the existence of two Pd species: Pd^0 [26,27] and Pd^{2+} [26,28]. The used catalysts exhibit also peaks due to Pd^0 and Pd^{2+} species, although the Pd^{2+}/Pd^0 ratio is much higher than for the fresh ones. This result suggests that the protons released during the reaction can oxidize Pd to Pd^{2+}. The increase of the Pd^{2+}/Pd ratio during hydrodechlorination reactions has been found by other authors in the literature in both gas and aqueous phase [29]. The unexpected (if the redox potentials for the H^+/Pd pair are considered) high stability of electron-deficient palladium species in reductive environments when chloride and protons ions are present in the solid has already been reported in the literature [30]. It is assumed that this behaviour is caused by the interaction of Pd^0 with neighbouring protons (arising from the HCl generated during the reaction in this case). The presence of chloride ions stabilizes this system, hence promoting the oxidation. This mechanism has been proposed in the literature for both hydrodechlorination reactions and explaining the abnormal reduction properties of catalysts prepared from chlorine-containing precursors [30].

XPS analyses of fresh catalysts reveal the presence of some chlorine from the Pd precursor. Although this precursor chlorine can promote catalyst sintering or poisoning, its contribution seems to be irrelevant in our case, because of the large amounts of HCl released during the reaction. After reaction, an important increase in the Cl/Pd ratio is observed in all cases, following the order: Pd/HSAG < Pd/AC < Pd/CNF. Two different Cl species are found on the surface of the used catalysts [29,31]: chloride anions, Cl $2p_{3/2}$, and chlorine covalently bonded to carbon (Table 2). According to the literature, inorganic chlorine can be formed by the reaction of the HCl released during the reaction with the Pd particles [32]. It is observed that the total amount of inorganic chlorine (calculated considering the Cl/Pd ration and the chlorine distribution reported in Table 2) increases for all the supports, being this increase much higher for the CNF-supported catalyst (three times vs. 50 and 70% increase for AC and HSAG, respectively). Concerning the concentration of organic chlorine, which is suggested to participate in the formation of coke [6,33], Pd/AC and Pd/CNF catalysts present an important increase in the percentage of Cl covalently bonded to C, catalysts in which the presence of coke was more important, as deduced from XRD and TPO.

4. Conclusions

The nature of the carbonaceous support has a relevant role in both the catalytic stability and the selectivity for the hydrodechlorination of TTCE over Pd supported catalysts. The Pd/HSAG catalyst has shown to be both the most stable and also the most selective to the total hydrodechlorination. For the Pd/activated carbon catalyst, the blockage of the micropores by the deposition of coke was aimed as the main deactivation cause; whereas for

Pd/CNF sintering of the active phase, as well as Pd oxidation (by the HCl released during the reaction) and coke fouling can affect the deactivation process. Concerning the Pd/HSAG catalyst, neither active phase sintering nor coke deposition was observed for the used catalyst, but oxidation of Pd^0 was observed as the main deactivation cause. The particular interactions between the palladium and the graphene surface, as well as the absence of microporosity and the presence of a certain amount of oxygenated surface groups could be the reason of the better behaviour of the HSAG-supported catalyst.

Acknowledgements

This work was supported by the Spanish Government (contract CTQ2005-09105-C04-04/PPQ). R.F. Bueres and E. Asedegbega-Nieto thank the Spanish Ministry of Science and Innovation for a Ph.D. fellowship and "Juan de la Cierva" program, respectively.

References

[1] U.S. Environmental Protection Agency, Integrated Risk Information System (IRIS) on Tetrachloroethylene, National Center for Environmental Assessment, Office of Research and Development, Washington, DC, 1999.
[2] Toxicological Profile for Trichloroethylene and Tetrachloroethylene, Agency for Toxic Substances and Disease Registry (ATSDR), Department of Health and Human Services, Public Health Service, Atlanta, GA, 1997.
[3] European Commission, Reference document on best available techniques for waste treatment, Seville, 2005, http://eippcb.jrc.es/pages/FActivities.htm.
[4] S. Ordoñez, F.V. Díez, H. Sastre, Appl. Catal. B 25 (2000) 49.
[5] S. Ordoñez, F.V. Díez, H. Sastre, Ind. Eng. Chem. Res. 41 (2002) 505.
[6] S. Ordoñez, F.V. Díez, H. Sastre, Appl. Catal. B 31 (2001) 113.
[7] S. Ordoñez, F.V. Díez, H. Sastre, Appl. Catal. B 40 (2003) 119.
[8] S. Ordóñez, H. Sastre, F.V. Díez, Thermochim. Acta 379 (2001) 25.
[9] C. Amorim, G. Yuan, P.M. Patterson, M.A. Keane, J. Catal. 234 (2005) 268.
[10] Q. Liu, Z.M. Cui, Z. Ma, S.W. Bian, W.G. Song, J. Phys. Chem. C 112 (2008) 1199.
[11] C. Liang, W. Xia, H. Soltani-Ahmadi, O. Schluter, R.A. Fischer, M. Muhler, Chem. Commun. (2005) 282.
[12] C. Pham-Huu, N. Keller, L.J. Charbonniere, R. Ziessel, M.J. Ledoux, Chem. Commun. (2000) 1872.
[13] R.F. Bueres, E. Asedgbega-Nieto, E. Díaz, S. Ordóñez, F.V. Díez, Catal. Commun. 9 (2008) 2080.
[14] E. Díaz, S. Ordóñez, A. Vega, J. Colloid Interface Sci. 305 (2007) 7.
[15] N. Krishnankutty, M.A. Vannice, J. Catal. 155 (1995) 312.
[16] C. Amorim, M.A. Keane, J. Colloid Interface Sci. 322 (2008) 196.
[17] M.A. Aramendia, R. Burch, I.M. Garcia, A. Marinas, J.M. Marinas, B.W.L. Southward, F.J. Urbano, Appl. Catal. B: Environ. 31 (2001) 163.
[18] P. Serp, M. Corrias, P. Kalck, Appl. Catal. A 253 (2003) 337.
[19] C. Park, M.A. Keane, J. Colloid Interface Sci. 266 (2003) 183.
[20] J.-P. Tessonnier, L. Pesant, G. Ehret, M.J. Ledoux, C. Pham-Huu, Appl. Catal. A 288 (2005) 203.
[21] M.R. Cuervo, E. Asedegbega-Nieto, E. Díaz, S. Ordóñez, A. Vega, A.B. Dongil, I. Rodríguez-Ramos, Carbon 46 (2008) 2096.
[22] M.R. Cuervo, E. Asedegbega-Nieto, E. Díaz, S. Ordóñez, A. Vega, E. Castillejos-López, I. Rodríguez-Ramos, J. Chromatogr. A 1188 (2008) 264.
[23] M.L. Toebes, Y. Zhang, J. Hajek, T.A. Nilhuis, J.H. Bitter, A.J. van Dillen, D.Y. Murzin, D.C. Koningsberger, K.P. de Jong, J. Catal. 226 (2004) 215.
[24] S.B. Ziemecki, G.A. Jones, J. Catal. 95 (1985) 621.
[25] S.B. Ziemecki, D.G. Schwarzfager, G.A. Jones, J. Am. Chem. Soc. 107 (1985) 4547.
[26] J.K. Murthy, S.C. Shekar, K.S.R. Rao, G. Kishan, J.W. Niemantsverdriet, Appl. Catal. A 259 (2004) 169.
[27] R. Gopinath, N. Lingaiah, B. Sreedhar, I. Suryanarayana, P.S. Sai Prasad, A. Obuchi, Appl. Catal. B 46 (2003) 587.
[28] G. Kumar, J.R. Blackburn, M.M. Jones, R.G. Albridge, W.E. Moddeman, Inorg. Chem. 11 (1972) 296.
[29] L. Gomez-Sainero, X.L. Seoane, J.L.G. Fierro, A. Arcoya, J. Catal. 209 (2002) 279.
[30] Z. Karpinski, Adv. Catal. 37 (1990) 45.
[31] L.E. Pimentel Real, A.M. Ferraria, A.M. Botelho do Rego, Polym. Test. 26 (2007) 77.
[32] X.L. Seoane, P.C. L'Argentiere, N.S. Fígoli, A. Arcoya, Catal. Lett. 16 (1992) 137.
[33] E. López, S. Ordóñez, F.V. Díez, Appl. Catal. B 62 (2006) 57.